Study of electrical properties with temperature variation by complex impedance spectroscopy (CIS) and effects on the Ba$_2$TiSi$_2$O$_8$–TiO$_2$ matrix

R. F. Abreu[1,2] · S. O. Saturno[1,2] · F. A. C. Nobrega[2,3] · D. da M. Colares[1,2] · J. P. C. do Nascimento[4] ·
S. J. T. Vasconcelos[2] · F. E. A. Nogueira[1,2] · D. B. de Freitas[6] · F. F. do Carmo[3] · A. Ghosh[5] · T. O. Abreu[2,3,11] ·
M. A. S. Silva[2] · R. S. Silva[6] · S. V. Trukhanov[7,8] · Di Zhou[9] · C. Singh[10] · A. S. B. Sombra[1,2]

Abstract

The present work shows the dielectric properties of (100-X)Ba$_2$TiSi$_2$O$_8$–(X)TiO$_2$ composites (X in wt%) at radio frequency (RF) region (< 300 MHz). X-ray diffraction and Rietveld's refinement showed the presence of Ba$_2$(Ti$_{7/9}$Si$_{2/9}$)$_9$O$_{20}$ (BTSO) phase in the studied composites. To analyze the relationship between the electrical properties and the microstructure of the matrix and composites, Impedance spectroscopy (IS) was used. The applied model that best describes the behavior found in the samples is the Havriliak–Negami model. From the IS it was observed that the dielectric relative permittivity presented high values in BTS10 ($X = 10\%$) and BTS20 ($X = 20\%$) which allows classifying them as Colossal permittivity materials. This is an important result due to the potential for applications in new storage systems, capacitive devices and microelectronics. Nyquist diagrams were employed to evaluate the contribution of the grain and grain boundary in the electrical response of the samples and fitted employing an equivalent circuit with two associations of R-CPE (constant phase element). Temperature coefficient of capacitance (TCC) was also obtained and it was possible to observe that there was an increase in the TCC value for the compounds in all frequencies. In addition, IS demonstrated that the activation energy decreasing with TiO$_2$ addition indicating a decrease in the resistive character of the materials.

Keywords Colossal permittivity · Ba$_2$TiSi$_2$O$_8$–TiO$_2$ composites · Impedance spectroscopy (IS)

✉ J. P. C. do Nascimento
jpquimico3@gmail.com

R. F. Abreu
roterdan.fernandes@gmail.com

1. Telecommunication Engineering Department, Federal University of Ceará (UFC), Fortaleza, Ceará 60755-640, Brazil

2. LOCEM-Telecommunication and Materials Science and Engineering of Laboratory (LOCEM)Physics Department, Federal University of Ceará (UFC), Campus PICI, P.O. Box 6030, Fortaleza, Ceará 60455-760, Brazil

3. Department of Organic and Inorganic Chemistry, Science Center, Federal University of Ceará (UFC), Fortaleza, Ceará, Brazil

4. Federal Institute of Education, Science and Technology of Ceará, PPGET, Fortaleza, Ceará, Brazil

5. Department of Chemical and Materials Engineering, DEQM, Pontifical Catholic University of Rio de Janeiro, Rio de Janeiro, Rio de Janeiro, Brazil

6. Group Functional Nanomaterials, Physics Department, Federal University of Sergipe, São Cristóvão, SE 49100-000, Brazil

7. Smart Sensors Systems Laboratory, National University, of Science and Technology MISiS, Moscow 119049, Russia

8. Laboratory of Magnetic Films Physics, Scientific Practical Materials Research Centre, NAS of Belarus, 220072 Minsk, Belarus

9. Electronic Materials Research Laboratory, Xi'an Jiaotong University, Xi'an 710049, China

10. School of Electronics and Electrical Engineering, Lovely Professional University, Phagwara, Punjab 144411, India

11. Instituto Federal de Educação, Ciência e Tecnologia do Ceará (IFCE), Campus Camocim, Camocim, CE 62400-000, Brazil

1 Introduction

Dielectric ceramics have been extensively studied due to their physical properties [1] which allow these materials to be used for different applications [1–3]. These materials, when endowed with a low dielectric loss combined with high values of permittivity and quality factor, are generally used in microwave circuits [1–3], while ceramics with low permittivity can be used in communication technology of fifth-generation (5G) [4]. In this technology, factors such as transmission speed and frequency are essential, which can be optimized by small values of the dielectric constant [4].

On the other hand, materials that have a colossal dielectric constant (CDC), that is, exhibit permittivities higher than 10^3, are fundamental for the miniaturization of electronic devices and allow for vast technological applications [5–10]. However, the electrical properties of a material depend on imperfections in its crystal lattice, porosity, particle size, etc. [1]. So, to characterize the electrical properties of ceramic materials, it is common to use impedance spectroscopy (IS) [11], which will be applied in this work focusing on the ceramic matrix $Ba_2TiSi_2O_8$ (BTS).

BTS is a rare silicate mineral that was discovered in Fresno County (USA) and its first reports date back to 1960 [1], it belongs to the space group P4bm [12–15], and has a non-center-symmetric tetragonal structure [16–18], due to its physical properties such as ferroelectricity [12, 15–17], pyroelectricity [12, 17, 19, 20], and piezoelectricity [19, 20] have attracted numerous studies on its structure, electrical properties, and possible technological applications.

This work sought to investigate the effect of the additions of 10%, 20%, 30%, and 40% by mass of TiO_2 in the pure phase of $Ba_2TiSi_2O_8$ on the electrical properties of BTS in the radiofrequency region through Spectroscopy Impedance (IS). It

is noteworthy that the choice of TiO_2 as an addition to the BTS phase is due to its technological applications in the radiofrequency (RF) region [20]. The structural characterization of the samples was carried out via X-ray diffraction (XRD), and the Rietveld refinement was used to confirm the phases. IS was used to study electrical properties varying the temperature from 380º to 460ºC and using a frequency spectrum of 1 Hz – 1 MHz. In this work, the following electrical parameters were studied: complex dielectric permittivity, capacitance temperature coefficient (TCC), conductivity and activation energy (E_a). The Nyquist diagram was used to identify and differentiate intrinsic effects (grains, grain boundaries) from extrinsic effects (electrode and interfacial effects).

2 Experimental procedure

For the preparation of the BTS matrix, the solid-state reaction was used following the stoichiometric proportions. In the synthesis, the following solid precursors were employed: $BaCO_3$ (99.99%, Vetec), TiO_2 anatase (99.8%, Aldrich), and SiO_2 (99.9%, Aldrich). The matrix was obtained according to the chemical equation (Eq. 1):

$$2BaCO_{3(s)} + 2SiO_{2(s)} + TiO_{2(s)} \rightarrow Ba_2TiSi_2O_{8(s)} + 2CO_{2(g)} \tag{1}$$
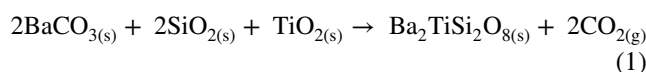
The high-energy mill with a rotation speed of 360 rpm for 4 h was used to grind the material. The resulting powder was calcined at 1100 °C for 6 h in a conventional oven. Subsequently, 10%, 20%, 30%, and 40% by mass of TiO_2 was added and mixed thoroughly to the BTS matrix using mortar, resulting in composites that were called BTS, BTS10, BTS20, BTS30, and BTS40, respectively. The prepared series are $(100-X)Ba_2TiSi_2O_8–(X)TiO_2$ composites (X in mass units). To produce the cylindrical disks the samples
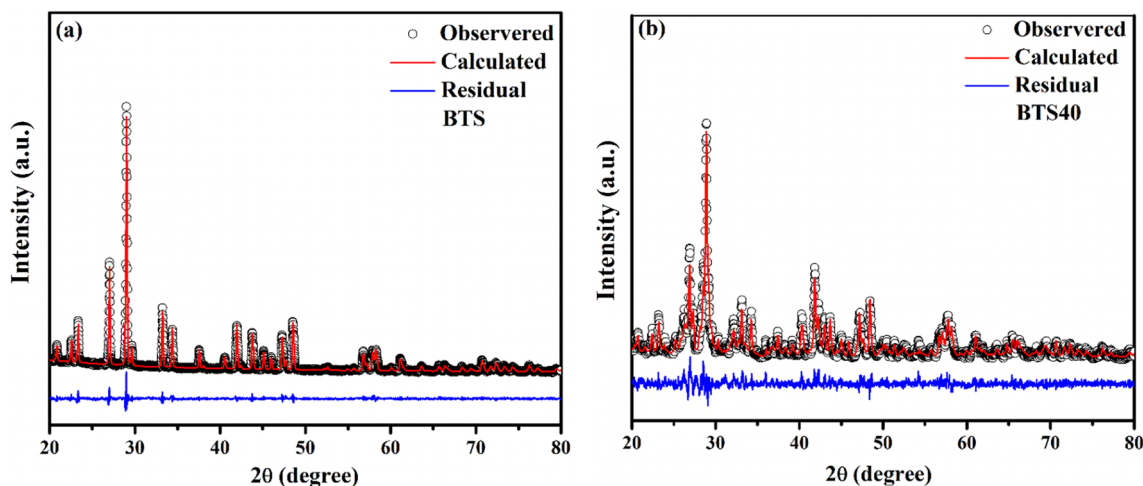

Fig. 1 Rietveld refinement of the: **a** BTS pure, and **b** BTS40 composite

were compacted via uniaxial pressure of 15.43 MPa. Finally, the pieces were sintered at 1200 °C for 4 h.

Through X-ray diffraction (XRD) the structures of the samples were analyzed. The Rigaku model D/max-B diffractometer with Cu cathode (Cu-Kα), 40 kV, 30 mA, and $\lambda = 1.5404$ Å, with an angular range in (2θ) of 20º–80º was used in this analysis. Using the Rietveld method and with the aid of the GSAS software, the phases obtained were confirmed and compared with the crystallographic sheets Inorganic Crystal Structure Database (ICSD) and Open Database of Crystallography (COD).

For the analysis of the electrical properties of the samples in RF, the ceramic discs had their faces covered with conductive silver paint to produce a capacitor. In this study, the conductivity and permittivity behavior are analyzed as a function of frequency with temperature variation to relate their macro and microscopic structures [21]. The temperature range used was 380º–460º C, with a frequency range of 1 Hz—1 MHz using the Impedance Analyzer (Solartron model 1260).

3 Results and discussion

3.1 X-ray diffraction

Figure 1a, b presents the Rietveld refinement of the powder XRD patterns of the BTS and BTS40 samples. Diffractogram obtained from BTS sample Fig. 1a demonstrate that peaks are well indexed to the tetragonal structure belonging to the P4bm space group (ICSD No. 15715) demonstrated that a single-phase was obtained.

In Fig. 1b, it is observed a significant change in the diffraction pattern of BTS40, where the presence of new diffraction peaks is observed, indicating that in addition to BTS and TiO$_2$, there is a new crystalline phase. Rietveld refinement confirmed the presence of the Ba$_2$(Ti$_{7/9}$Si$_{2/9}$)$_9$O$_{20}$ (BTSO) phase in all composites and demonstrates that there was a reaction between BTS and TiO$_2$. The formation reaction of the BTSO phase is shown in Eq. (2):

$$Ba_2TiSi_2O_{8(s)} + 6\ TiO_{2(s)} \rightarrow Ba_2\left(Ti_{7/9}Si_{2/9}\right)_9O_{20(s)} \quad (2)$$
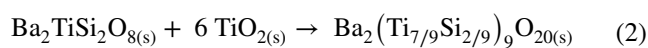
Statistical parameters and mass fractions obtained from Rietveld refinement for all materials are presented in the Table 1. As observed in the BTS10 and BTS20 composites, all TiO2 added was reacted completely forming the BTSO phase, whereas a certain percentage of TiO$_2$ remained in the compositions BTS30 and BTS40.

3.2 RF analysis

Impedance spectroscopy is an extremely powerful technique that allows analyzing the electrical behavior of materials and obtaining important information about the structure of the material, its electrical nature, conduction mechanisms, etc. [10, 22, 23]. To analyze the electrical and dielectric properties, BTS and composites impedance spectroscopy is utilized from the frequency spectrum of 1 Hz–1 MHz and varying the temperature from 380º to 460º C. The complex dielectric permittivity can be written mathematically according to Eq. (3):

$$\varepsilon_r^* = \varepsilon' - j\varepsilon_r'', \quad (3)$$

where the real component of dielectric permittivity (ε'_r) represents energy storage, whereas the imaginary one (ε''_r) represents all losses [21, 24]. The model that showed the best compatibility to analyze the effects of increasing frequency with temperature variation on the behavior of ε'_r was the Havriliak–Negami model [21, 22, 25], described in Eq. (5).

$$\varepsilon_r^* = \varepsilon_{r\infty} + \frac{(\varepsilon_{rs} - \varepsilon_{r\infty})}{\left[1 + (j\omega\tau)^{1-\alpha}\right]^\beta}. \quad (4)$$

$$\varepsilon_r' = \varepsilon_{r\infty} + \frac{\cos\beta\phi}{r^\beta} \cdot \left(\varepsilon_{rs} - \varepsilon_{r\infty}\right) \quad (5)$$

$$\varepsilon_r'' = \frac{\mathrm{sen}\beta\phi}{r^\beta} \cdot \left(\varepsilon_{rs} - \varepsilon_{r\infty}\right) \quad (6)$$

Table 1 Statistical parameters and mass fractions obtained through Rietveld refinement for composites

	Statistical parameters			Mass fraction (%)			d_{relative} (%)
	R_{WP} (%)	χ^2	R_{bragg} (%)	Ba$_2$TiSi$_2$O$_8$	Ba$_2$(Ti$_{7/9}$Si$_{2/9}$)$_9$O$_{20}$	TiO$_2$	
BTS	5.84	1.679	4.93	100	–	–	92.81
BTS10	11.13	1.979	6.53	79.60	20.40	–	94.94
BTS20	10.47	1.877	6.47	71.07	28.93	–	92.29
BTS30	10.96	2.061	5.79	48.67	48.27	3.06	91.30
BTS40	16.06	1.564	9.28	31.31	62.03	6.66	90.61

ε_{rs} relative static permittivity, $\varepsilon_{r\infty}$ relative permittivity for high frequencies ($\omega \to \infty$), ω is the natural frequency of angular oscillation, and τ it's relaxation time. The values of α and β belong to the intervals $0 < \alpha < 1$e $0 < \beta < 1$.

In Fig. 2, the ε'_r curves of all samples at room temperature are presented, through which it can be seen that samples BTS10 and BTS20 exhibit values well above 10^3, which demonstrate that these samples have colossal permittivities [23, 24]. Since BTS has a low permittivity value at room temperature [28, 29], the elevated values obtained for these composites could be explained due to presence to the BTSO phase indicating that this phase has colossal permittivity. These results obtained are interesting since they would allow to reduce the geometric measurements of capacitive components, applications such as random access memories, energy storage, multifunctional electronic devices, and sensors [5–9, 26]. The effect of temperature variation on permittivity in the range of 380–460 ºC is presented in the Supplementary Material.

Figure 3 a–e shows the imaginary impedance spectra (Z'') by frequency at different temperatures. It is possible to observe that the Z'' peak moves to high frequencies with increasing temperature, this fact indicates a thermally activated process [30–32]. The asymmetry of the peaks and their broadening indicates the non-Debye nature of the samples this fact agrees with Eq. (4) [31, 33]. The influence of the temperature variation on real impedance (Z') is showed in the Supplementary Material.

The effect of conductivity at different temperatures is shown in Fig. 4a, b, whereas it is observed that conductivity increases with temperature variation, confirming a thermally

activated process [30, 36]. The universal power law, Eq. (7), describes the behavior of the samples [38–40].

$$\sigma_{\text{total}}(\omega) = \sigma_{\text{DC}} + A\omega^n, \tag{7}$$

σ_{DC} is the DC conductivity; A it is thermally activated quantity; n is an exponent with variation $0 < n < 1$.

Moreover, it is possible to observe that the increase in conductivity as a function of frequency occurs exponentially, obeying the power law, $\sigma(\omega) \, \alpha \, \omega^n$ mentioned previously. In this way, the value of n expresses the physical meaning of the type of jump manifested by the charge carriers. That is, when $0 < n < 1$ it means that the carriers present a translational jump movement with a sudden jump, while when $n > 1$ it means that the movement of the charge carriers involves a localized jump without them leaving the neighborhood [30, 33, 41]. Table 2 presents the values of σ_{DC}, A, n, and R^2. Observing Figure and the results obtained in table, it is valid to infer for all samples that the movement of charge carriers involves translational jump movement with a sudden jump.

In Eq. (8) and (9) the Arrhenius relation was used to calculate the activation energy of the samples, whereas was employed values of σ' and Z''.

$$\sigma' = \sigma_0 \prime \cdot e^{-E_a/kT} \tag{8}$$

$$f_{\text{max}} = f_0 \cdot e^{-E_a/kT} \tag{9}$$

σ_0 and f_0 are the constant pre-exponential factor; f_{max} is the maximum frequency of Z''; E_a is the activation energy of the mobile charge carriers; k is the Boltzmann constant; T the temperature in Kelvin.

In the Fig. 5a–e and Table 3, it is possible to notice that the values of activation energy calculated by Z'' and σ' are close indicating that the same charge carriers are involved in the conduction process. Moreover, E_a decrease with the increase of TiO_2 addition, with BTS demonstrating the highest value of activation energy, whereas BTS40 presents the lowest value. This fact could be explained due to the presence of the BTSO and TiO_2 phases in the composites, it is emphasized that the TiO_2 has a lower activation energy than the BTS phase [42].
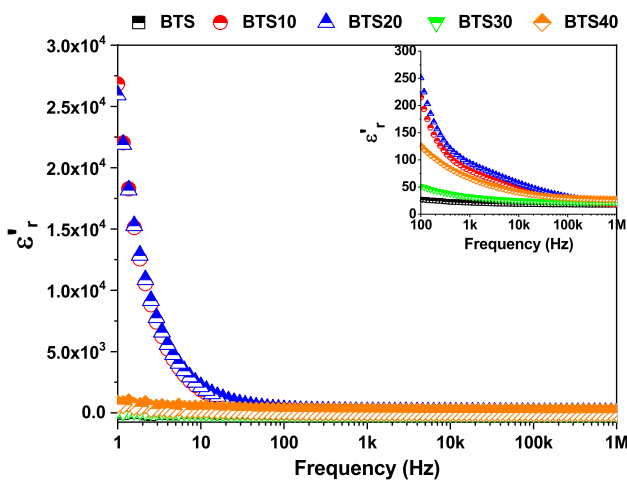
4 Nyquist analysis

To study the effects of grains, grain boundaries, and electrode effects, the Nyquist diagram was used. Thus, for modeling the equivalent circuits in each sample, the R (resistor) and CPE (constant phase element) elements were used.
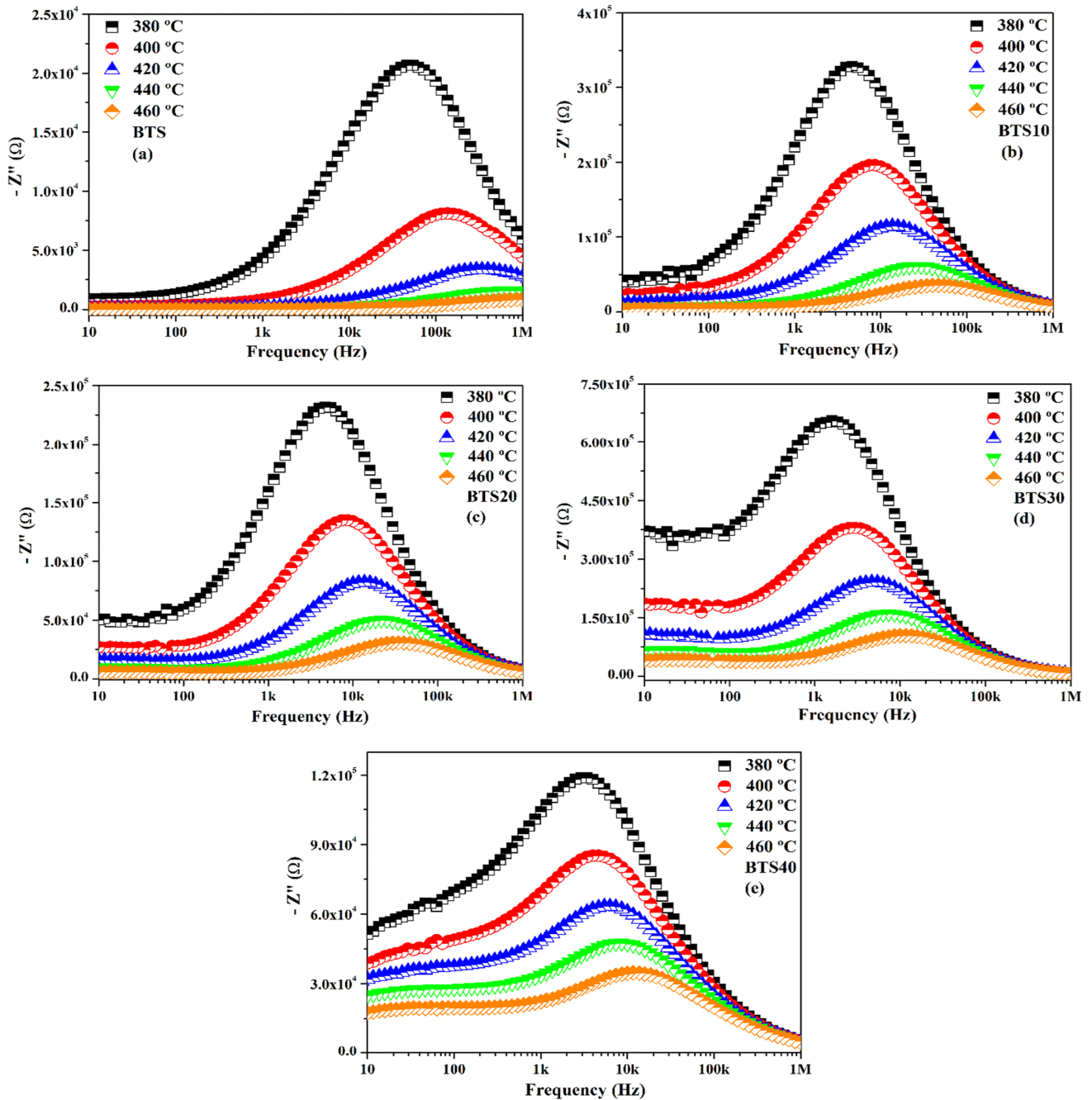

Fig. 2 Dielectric permittivity $Ba_2TiSi_2O_8$ and composites at room temperature

Fig. 3 **a–e** Z'' spectrum as a function of temperature for all samples

The CPE can be used in different ways within an electrical circuit assuming inductor, resistor or capacitor functions depending on the values of n ($n = -1, 0, 1$), respectively [34]. All curves were plotted using an equivalent circuit composed of two parallel R-CPE associations (see Fig. 6a) that are related to grain and grain boundary effects. Equation (10) allows calculating the impedance of the CPE,

$$Z_{CPE}(\omega) = q^{-1} \cdot (j\omega)^{-n}, \tag{10}$$
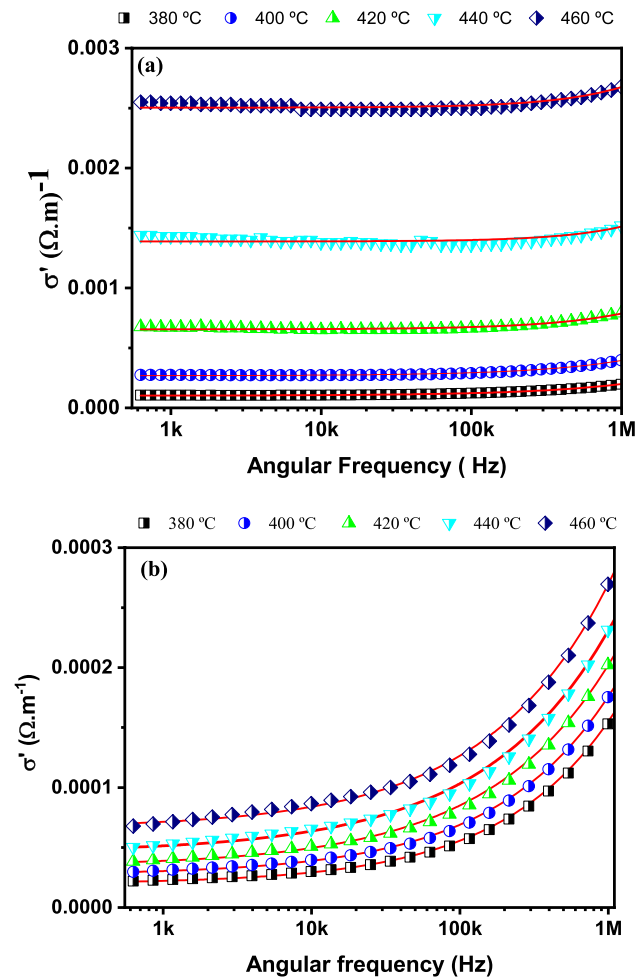
where q is the proportionality factor.

Fig. 4 Conductivity spectrum at different temperatures of **a** BTS and **b** BTS40

Table 2 Fitting parameters of Jonscher's power law for all samples in AC conductivity

Temperature (°C)	σ_{DC} (S/cm³)	A	n	R^2
BTS				
380	1.02×10^{-4}	8.63×10^{-9}	0.675	0.998
400	2.68×10^{-4}	7.08×10^{-9}	0.709	0.999
420	6.55×10^{-4}	1.29×10^{-9}	0.835	0.995
440	1.39×10^{-3}	1.35×10^{-10}	0.994	0.978
460	2.50×10^{-3}	3.42×10^{-10}	0.950	0.992
BTS10				
380	1.24×10^{-5}	1.51×10^{-10}	0.886	0.999
400	1.91×10^{-5}	3.05×10^{-10}	0.853	0.994
420	3.09×10^{-5}	7.72×10^{-10}	0.803	0.996
440	5.58×10^{-5}	1.73×10^{-10}	0.763	0.998
460	9.29×10^{-5}	9.29×10^{-9}	0.746	0.999
BTS20				
380	1.33×10^{-5}	1.71×10^{-9}	0.735	0.99
400	2.21×10^{-5}	2.08×10^{-9}	0.739	0.99
420	3.52×10^{-5}	3.56×10^{-9}	0.715	0.99
440	5.45×10^{-5}	1.74×10^{-8}	0.619	0.99
460	8.93×10^{-5}	2.15×10^{-8}	0.617	0.99
BTS30				
380	6.68×10^{-6}	7.46×10^{-11}	0.916	0.997
400	9.75×10^{-6}	2.83×10^{-10}	0.839	0.998
420	1.32×10^{-5}	1.56×10^{-9}	0.734	0.999
440	1.91×10^{-5}	2.42×10^{-9}	0.716	0.995
460	2.83×10^{-5}	3.57×10^{-9}	0.702	0.997
BTS40				
380	1.96×10^{-5}	4.80×10^{-8}	0.575	0.998
400	2.71×10^{-5}	7.46×10^{-8}	0.550	0.997
420	3.42×10^{-5}	1.30×10^{-7}	0.518	0.998
440	4.59×10^{-5}	1.64×10^{-7}	0.508	0.998
460	6.60×10^{-5}	1.39×10^{-7}	0.527	0.999

The equivalent impedance of each loop (R-CPE) can be calculated according to Eq. (11),

$$\frac{1}{Z(\omega)} = \frac{1}{R} + q(j\omega)^n \Rightarrow$$

$$Z(\omega) = \frac{R + qR^2\omega^n \cos\left(\frac{n\pi}{2}\right)}{1 + 2Rq\omega^n \cos\left(\frac{n\pi}{2}\right) + R^2q^2\omega^{2n}} - j\frac{qR^2\omega^n \text{sen}\left(\frac{n\pi}{2}\right)}{1 + 2Rq\omega^n \cos\left(\frac{n\pi}{2}\right) + R^2q^2\omega^{2n}}. \tag{11}$$

The equivalent impedance will be the sum of the impedances calculated according to Eq. (8) [35]. According to Fig. 6a–e it is possible to observe that the increase in temperature causes the attenuation of the curves—Z'' (Ω) × Z' (Ω). Table 4 presents the data obtained in the adjustments, whereas R_g, P_g, R_{gb} and P_{gb} refer to grain resistance, grain capacitance, grain boundary resistance and grain boundary resistance capacitance, respectively.

According to Table 4, it was possible to observe that the value of n in the grains, in all samples was approximately between $0.8 \leq n < 1$, and in this case the CPE represents a capacitance distortion caused by the accumulation / distribution of charge carriers or by the roughness of the
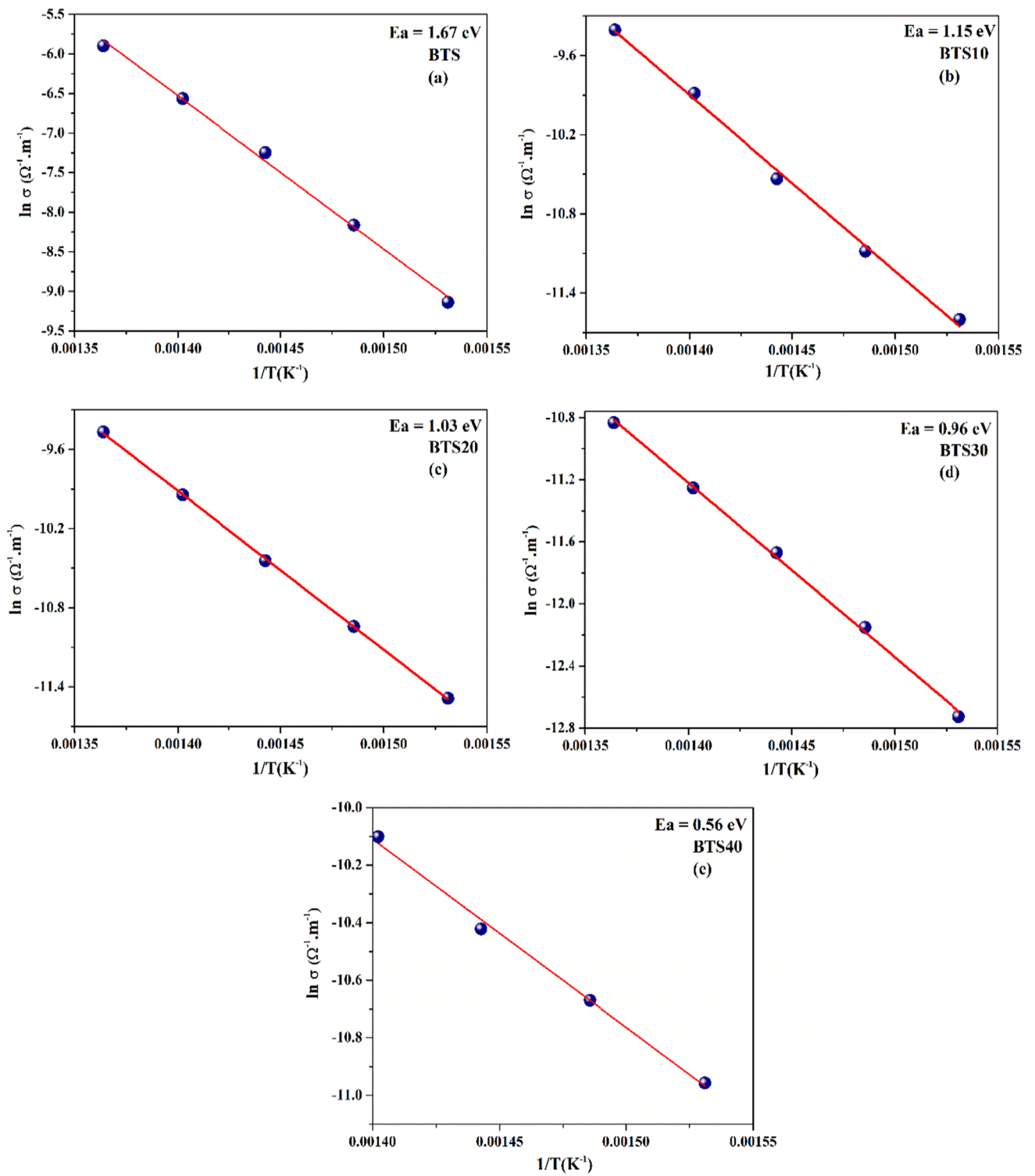
Fig. 5 **a–e** Activation energy obtained through the conductivity

Table 3 Activation energy obtained by σ' and Z''

Sample	E_a/σ' (eV)	E_a/Z'' (eV)
BTS	1.67	1.68
BTS10	1.15	1.20
BTS20	1.03	1.01
BTS30	0.96	0.95
BTS40	0.56	0.63

electrode surface [35]. Regarding the grain boundary, the BTS sample showed the behavior indicated above for temperatures 380º–400 ºC, while at temperatures 420º–460 ºC, the contribution of the grain boundary was in the range of $0.4 < n \leq 0.6$, and in this range the CPE indicates diffusion effects with deviations from Fick's second law [35]. All composites presented grain boundary values of $0.4 < n \leq 0.6$ in the range of 380º–460 ºC, and again

the CPE is related to the previously mentioned diffusion effects [35].

Finally, it should be noted that the increase in temperature causes a decrease in the values of the grain boundary resistances in all the samples studied, and this effect favors the conduction process, as it facilitates the movement of charge carriers within the samples, which behavior is related to potential barrier lowering [30].

4.1 TCC (temperature coefficient of capacitance)

With the objective of evaluating the behavior of the capacitance variation of the material from the increase in temperature, the study of the temperature coefficient of capacitance (TCC) was used [30]. It is worth mentioning that the TCC close to zero is a relevant factor for the miniaturization of capacitive electronic devices [3, 26].

Table 4 Adjustment of equivalent circuit parameters from 380 to 460 ºC for all samples

| Temperature (ºC)	Grain			Grain boundary		
	R_g (Ω)	P_g (F)	n_g	R_{gb} (Ω)	P_{gb} (F)	n_{gb}
BTS						
380	31,159	5.4568×10^{-10}	0.8192	32,634	3.0396×10^{-9}	0.77997
400	2402.2	5.2955×10^{-9}	0.93526	22,210	1.1632×10^{-9}	0.7608
420	9000	1.7791×10^{-9}	0.75807	1393.9	1.7191×10^{-7}	0.54682
440	4090.2	2.153×10^{-9}	0.76179	1047.9	1.7203×10^{-6}	0.40941
460	2000	1.7488×10^{-9}	0.80304	688.62	3.3880×10^{-7}	0.47772
BTS10						
380	9.1854×10^5	3.3979×10^{-10}	0.78618	1.7025×10^5	7.9735×10^{-10}	0.46965
400	5.5088×10^5	3.8393×10^{-10}	0.78482	1.0039×10^5	1.1278×10^{-6}	0.45606
420	3.1994×10^5	4.1495×10^{-10}	0.78777	55,731	2.4167×10^{-6}	0.42845
440	1.6937×10^5	4.4978×10^{-10}	0.79099	27,299	4.0113×10^{-6}	0.42183
460	99,916	5.2410×10^{-10}	0.78843	23,876	7.6534×10^{-6}	0.38404
BTS20						
380	6.5378×10^5	5.1950×10^{-10}	0.77694	2.3692×10^5	8.5551×10^{-7}	0.45817
400	3.8169×10^5	5.8106×10^{-10}	0.77748	1.3212×10^5	1.446×10^{-6}	0.45376
420	2.3251×10^5	6.4278×10^{-10}	0.77883	78,702	2.3072×10^{-6}	0.45072
440	1.4085×10^5	7.1858×10^{-10}	0.77915	47,706	3.6634×10^{-6}	0.44487
460	86,664	8.0459×10^{-10}	0.77886	30,690	5.7938×10^{-6}	0.43456
BTS30						
380	1.7307×10^6	4.3263×10^{-10}	0.77766	1.7336×10^6	1.2315×10^{-7}	0.4848
400	1.0000×10^6	4.2373×10^{-10}	0.788	8.6167×10^5	1.8955×10^{-7}	0.47816
420	6.4912×10^5	4.6248×10^{-10}	0.78558	4.7542×10^5	2.8347×10^{-7}	0.48905
440	4.3078×10^5	4.8083×10^{-10}	0.78847	2.9428×10^5	3.7743×10^{-7}	0.49393
460	2.8274×10^5	5.1831×10^{-10}	0.78971	1.8901×10^5	5.0459×10^{-7}	0.49681
BTS40						
380	3.1949×10^5	2.099×10^{-9}	0.72498	2.4497×10^5	2.9841×10^{-7}	0.47594
400	2.3067×10^5	2.3298×10^{-9}	0.72169	1.9127×10^5	3.9098×10^{-7}	0.46893
420	1.7407×10^5	2.6283×10^{-9}	0.71652	1.6282×10^5	5.1091×10^{-7}	0.46046
440	1.3189×10^5	2.8597×10^{-9}	0.71381	1.3168×10^5	7.2026×10^{-7}	0.4475
460	9.7301×10^4	2.9272×10^{-9}	0.71509	9.5431×10^4	9.8801×10^{-7}	0.44095
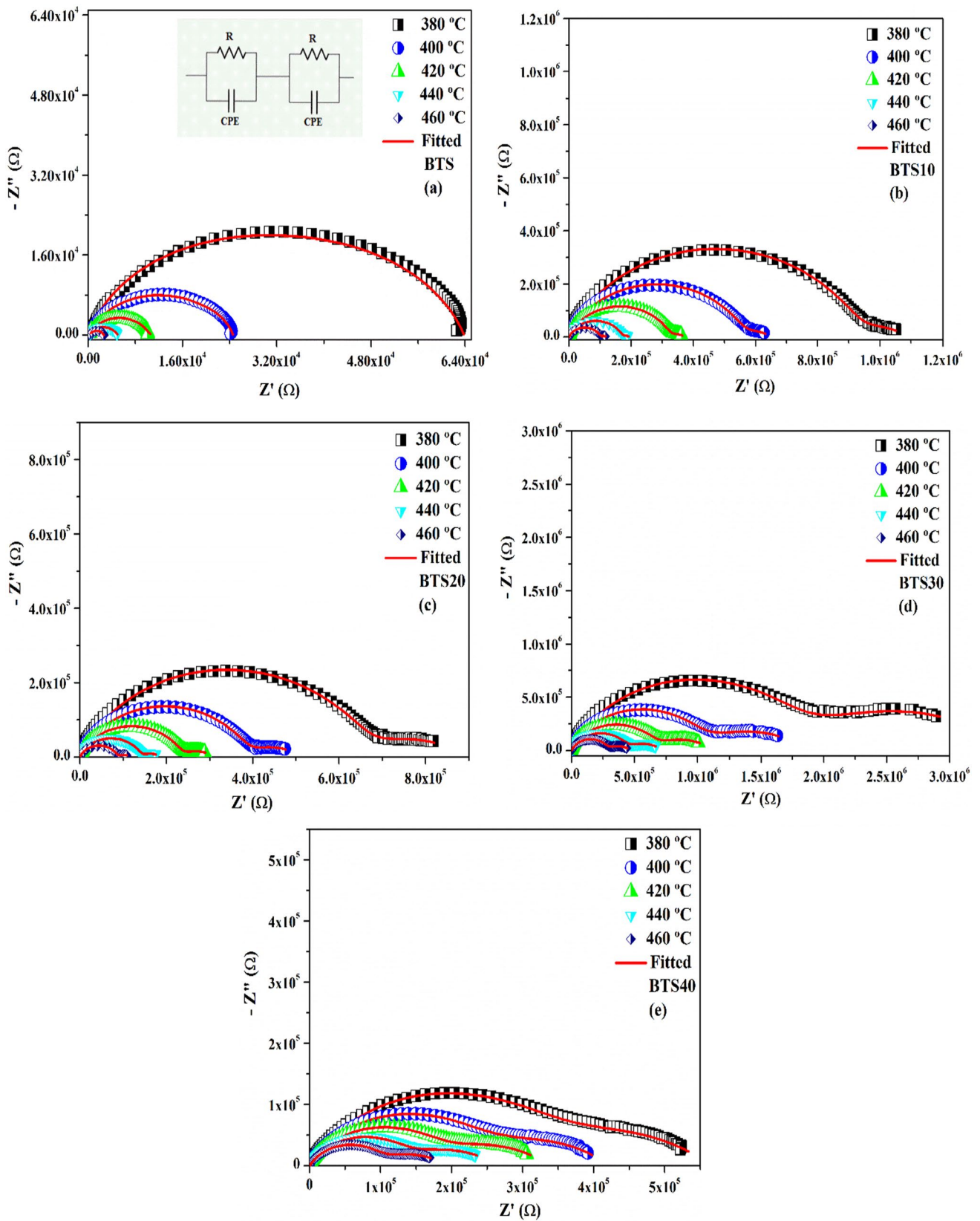
Fig. 6 A—e)—Z" x Z' spectrum as a function of temperature for all samples

Table 5 TCC values for the $Ba_2TiSi_2O_8$ and composites at different frequencies

TCC (ppm/ºC)

Frequency	BTS	BTS10	BTS20	BTS30	BTS40
10 Hz	− 5716.78	− 12,381.86	− 13,391.75	− 8713.21	− 8642.40
100 Hz	− 6006.36	− 7328.33	− 10,914.51	− 6272.63	− 5337.93
1 kHz	− 6008.54	− 6307.03	− 9257.66	− 3189.025	− 1693.09
10 kHz	− 5044.15	− 6433.48	− 8361.93	− 1315.17	+ 562.79
100 kHz	− 5552.38	− 4012.46	− 5333.34	− 450.67	+ 320.04
1 MHz	− 10,146.51	− 1116.14	− 1891.06	+ 16.34	− 58.00

Table 5 shows the TCC results of BTS and composites, calculated from 10 Hz to 1 MHz. It is possible to see that the TiO_2 additions cause an increase in the thermal stability in the BTS30 and BTS40 samples since TCC values close to zero were obtained. For BTS30 and BTS40, it is expected to obtain TCC = 0 in the range between 100 kHz and 1 MHz. These values are important in the miniaturization of electronic devices, and therefore, it can be inferred that the addition of TiO_2 caused an increase in the thermal stability of the composites.

5 Conclusion

This work presents a study of the electrical properties of the ceramic matrix $Ba_2TiSi_2O_8$ with additions of TiO_2 (100-X) $Ba_2TiSi_2O_8$ – (X)TiO_2 composites (X in mass units) in the radiofrequency region. X-ray diffraction and Rietveld's refinement demonstrated the formation of $Ba_2(Ti_{7/9}Si_{2/9})_9O_{20}$ (BTSO) phase in the composites. The study of the electrical properties of the samples was carried out using impedance spectroscopy, where it was observed that the dielectric relative permittivity (ε'_r) presented colossal values for samples BTS10 ($X = 10\%$) and BTS20 ($X = 20\%$) and the relaxation phenomenon is consistent with the model of Havriliak–Negami. Through the analysis of the dielectric permittivity and impedances, it was possible to perceive that the relaxation effects observed in the samples may have been caused Maxwell–Wagner mechanism. The study of the temperature coefficient of capacitance (TCC) was carried out and the sample of BTS30 presented the value closest to the range for applications in capacitive components. Regarding the activation energy, a decrease in its value was noticed with the increase of TiO_2 additions.

Declarations

Conflict of interest The authors declare that they have no conflict of interest.

References

1. M.T. Sebastian, *Dielectric Materials for Wireless Communication* (Elsevier Science, 2008)
2. L.F. Chen, C.K. Ong, C.P. Neo, V.V. Varadan, V.K. Varadan, *Microwave Electronics: Measurement and Materials Characterization* (Wiley, 2004)
3. A.J. Moulson, J.M. Herbert, *Electroceramics: Materials, Properties, Applications* (Wiley, Chichester, 2003)
4. C. Yin, Z. Yu, L. Shu, L. Liu, Y. Chen, C. Li, J. Adv. Ceram. **10**, 108 (2021)
5. J. Sun, R. Ahmed, G.J. Wang, S.T. Wang, J. Wang, S.A. Suhaib, Y.M. Xie, H. Bi, C.C. Wang, J. Mater. Sci. **54**, 6323 (2019)
6. N. Humera, S. Riaz, N. Ahmad, F. Arshad, R. Zafar, S. Ali, S. Idrees, H. Noor, S. Atiq, and S. Naseem, J. Mater. Sci. Mater. Electron. (2020).
7. Y. Wang, W. Jie, C. Yang, X. Wei, J. Hao, Adv. Funct. Mater., p. 1808118 (2019).
8. J. Zheng, Q. Fu, X. Chen, C. Chakrabarti, P. Wang, H. Yin, C. Li, Y. Qiu, S. Yuan, J. Mater. Sci. Mater. Electron. **32**, 290 (2021)
9. Z. Wang, P. Peng, L. Zhang, N. Wang, B. Tang, B. Cui, J. Liu, D. Xu, J. Mater. Sci. Mater. Electron. **33**, 6283 (2022)
10. Y. Song, P. Liu, B. Guo, X. Cui, W. Yang, J. Am. Ceram. Soc. **103**, 4313 (2020)
11. E. Barsoukov, J.R. Macdonald, *Impedance Spectroscopy*, 3rd edn. (Wiley, Hoboken, 2018)
12. Q. Shi, T.-J. Park, J. Schliesser, A. Navrotsky, B.F. Woodfield, J. Chem. Thermodyn.Thermodyn. **72**, 77 (2014)

13. S. Cao, B. Jiang, Y. Zheng, X. Tu, K. Xiong, P. Gao, E. Shi, J. Cryst. GrowthCryst. Growth **451**, 207 (2016)
14. C. Shen, H. Zhang, D. Wang, J. Wang, R.I. Boughton, Crystals (2017)
15. M. Sahu, S. Mukherjee, M. Keskar, K. Krishnan, S. Dash, B.S. Tomar, Thermochim. Acta. Acta **663**, 215 (2018)
16. E.E. Abbott, M. Mann, J.W. Kolis, J. Solid State Chem. **184**, 1257 (2011)
17. S.K. Barbar, M. Roy, J. Mol. Struct.Struct. **1024**, 132 (2012)
18. C. Jiang, F. Chen, F. Yu, S. Tian, X. Cheng, S. Zhang, X. Zhao, Crystals **9**, 11 (2019)
19. S. Weber, A. Lebedinskaya, D. Rudsky, Y. Kabirov, A. Rudskaya, M. Kupriyanov, J. Adv. Dielectr. (2020).
20. J.A.R. Lopez, L.M.A. Silva, H. Leon-Leon, M. Valverde-Alva, L. Korotkov, E. Rysiakiewicz-Pasek, N. Emelianov, AIP Conf. Proc., p. 050002 (2020)
21. A.J. Vadim, F. LvovichWiley, *Impedance Spectroscopy: Applications to Electrochemical and Dielectric Phenomena* (Wiley, 2012)
22. J. Shukla, P. Saxena, P. Joshi, P. Joshi, A. Mishra, Appl. Phys. A **129**, 731 (2023)
23. R.K. Veena, A. Anand, M. Manjuladevi, V.S. Veena, J. Cyriac, N. Kalarikkal, S. Sagar, Appl. Phys. A. Phys. A **129**, 598 (2023)
24. K.C. Kao, *Dielectric Phenomena in Solids* (Elsevier Science, 2004)
25. S. Havriliak, S. Negami, Polymer (Guildf). **8**, 161 (1967)
26. P. Lunkenheimer, V. Bobnar, V. Bobnar, A.V. Pronin, A. V. Pronin, A.I. Ritus, A.A. Volkov, A. Loidl, Phys. Rev. B-Condens. Matter Mater. Phys. (2002).
27. M. Idrees, M. Nadeem, M. Atif, M. Siddique, M. Mehmood, M.M. Hassan, Acta Mater. (2011).
28. R.F. Abreu, T.O. Abreu, D.M. da Colares, S.O. Saturno, J.P.C. do Nascimento, F.A.C. Nobrega, A. Ghosh, S.J.T. Vasconcelos, J.C. Sales, H.D. de Andrade, I.S.Q. Júnior, A.S.B. Sombra, J. Mater. Sci. Mater. Electron.. Mater. Sci. Mater. Electron. **32**, 7034 (2021)
29. J. Shen, J. Zhou, X. Cui, L. Li, J. Electroceramics **21**, 565 (2008)
30. B. Behera, P. Nayak, R.N.P. Choudhary, J. Alloys Compd. **436**, 226 (2007)
31 K.C. VaradaRajulu, B. Tilak, K. Sambasiva Rao, Appl. Phys. A **106**, 533 (2012)
32. B.C. Sutar, R.N.P. Choudhary, P.R. Das, Ceram. Int. **40**, 7791 (2014)
33. D.K. Kushvaha, B. Tiwari, S.K. Rout, J. Alloys Compd. **829**, 154573 (2020)
34. A. Lasia, Electrochemical Impedance Spectroscopy and Its Applications (2014)
35. X.-Z. Yuan, C. Song, H. Wang, J. Zhang, *Electrochemical Impedance Spectroscopy in PEM Fuel Cells* (Springer London, London, 2010)
36. R.F. Abreu, F.A.C. Nobrega, D.M. da Colares, S.O. Saturno, J.P.C. do Nascimento, T.O. Abreu, A. Ghosh, F.F. Carmo, M.A.S. Silva, A.J.M. Sales, R.S. Silva, A.S.B. Sombra, J. Mater. Sci. Mater. Electron.. Mater. Sci. Mater. Electron. **34**, 457 (2023)
37. C. Karthik, K.B.R. Varma, J. Phys. Chem. Solids **67**, 2437 (2006)
38. A.K. Jonscher, J. Phys. D Appl. Phys. **32**, R57 (1999)
39. T. Acharya, R.N.P. Choudhary, J. Electron. Mater. (2015).
40. T. Acharya, R.N.P. Choudhary, Phys. Lett. A **380**, 2437 (2016)
41. K. Funke, Prog. Solid State Chem.. Solid State Chem. **22**, 111 (1993)
42. M.A.S. Silva, R.G.M. Oliveira, A.S.B. Sombra, Ceram. Int. **45**, 20446 (2019)